

本文章已註冊DOI數位物件識別碼

▶ Wide Area Differential GNSS in Taiwan: Development and Validation Testing

doi:10.6125/JoAAA.201012_42(4).07

Journal of Aeronautics, Astronautics and Aviation. Series A, 42(4), 2010

航空太空及民航學刊, 42(4), 2010

作者/Author : An-Lin Tao;Li-Ta Hsu;Shau-Shiun Jan

頁數/Page : 259-267

出版日期/Publication Date :2010/12

引用本篇文獻時，請提供DOI資訊，並透過DOI永久網址取得最正確的書目資訊。

To cite this Article, please include the DOI name in your reference data.

請使用本篇文獻DOI永久網址進行連結:

To link to this Article:

[http://dx.doi.org/10.6125/JoAAA.201012_42\(4\).07](http://dx.doi.org/10.6125/JoAAA.201012_42(4).07)



DOI Enhanced

DOI是數位物件識別碼 (Digital Object Identifier, DOI) 的簡稱，是這篇文章在網路上的唯一識別碼，用於永久連結及引用該篇文章。

若想得知更多DOI使用資訊，

請參考 <http://doi.airiti.com>

For more information,

Please see: <http://doi.airiti.com>

請往下捲動至下一頁，開始閱讀本篇文獻

PLEASE SCROLL DOWN FOR ARTICLE



Wide Area Differential GNSS in Taiwan: Development and Validation Testing*

An-Lin Tao, Li-Ta Hsu, and Shau-Shiun Jan**

*Department of Aeronautics and Astronautics, National Cheng Kung University
No.1, Ta-Hsueh Road, Tainan 701, Taiwan, R.O.C.*

ABSTRACT

To provide the enhanced Global Navigation Satellite System (GNSS) service in Taiwan, a Satellite Based Augmentation System (SBAS) prototype, the Wide Area Differential GNSS (WADGNSS), is developed and tested in this work in order to facilitate the implementation and operation of a SBAS and to evaluate its services to support the land and maritime transportations in Taiwan. There are three major components of a WADGNSS, namely one Test-bed Master Station (TMS), several L1-L2 dual-frequency Test-bed Reference Stations (TRSSs), and the WADGNSS user equipment. This paper will focus on the development and validation of the TMS and TRSSs. In this work the e-GPS satellite tracking stations which are originally designed for the surveying and mapping purposes will be used as our TRSSs; therefore, the difficulties and challenges to use them as the WADGNSS TRSSs will be investigated. The data processes and communications between the TRSSs and TMS will be investigated in this work, and the detailed development steps of the TMS and their validation testing will be discussed in this paper as well. Finally, the performance of the developed WADGNSS is presented by comparing the positioning results with standalone GPS measurement and that using WADGNSS correction messages. Based on the results presented in this work, the performance of the GPS users in Taiwan could be enhanced by applying the WADGNSS correction message.

Keywords: GPS, WADGNSS, Integrity

I. INTRODUCTION

As the increasing needs of the global market, several countries have been involving to develop the Global Navigation Satellite System (GNSS), which includes the United States' Global Positioning System (GPS), European Galileo, Russian Global Navigation Satellite System (GLONASS) and Chinese Beidou Satellite Navigation and Positioning system. That is, the applications of GNSS are getting more comprehensive. Most applications require a reliable positioning and navigation service. Unfortunately, the stand alone GNSS positioning service cannot support the safety-of-life applications. As illustrated by the civil

aviation and maritime applications, a navigation system is regulated to satisfy the Required Navigation Performance (RNP) in terms of four requirements: accuracy, integrity, continuity and availability [1]. In some cases, the GNSS positioning results may lead to a Hazardously Misleading Information (HMI), and it means that the actual errors of positioning results are greater than the calculated Protection Level (PL) [1]. This misleading information may cause accidents when the detrimental GPS signal is received by users. To solve this problem, a GNSS augmentation system is developed in this paper to improve the GNSS performance and it is called the Wide Area Differential GNSS (WADGNSS). This WADGNSS is developed for

* This paper was presented in "International Symposium on GPS/GNSS 2010", Taipei, Taiwan on October 25-28, 2010, and is recommended by the Symposium General Committee. Final manuscript is accepted on December 06, 2010.

** To whom correspondence should be addressed, E-mail: ssjan@mail.ncku.edu.tw

Taiwan region to provide a high integrity GNSS positioning service. In Asia, the MSAS is successfully developed and operated and the GPS Aided Geo Augmented Navigation (GAGONS) is under development phase. However, there might be a service gap in Asia near Taiwan region as shown in Figure 1. If there is a GNSS augmentation system in Taiwan, it will be helpful to complement the integrity GNSS service in Asia.

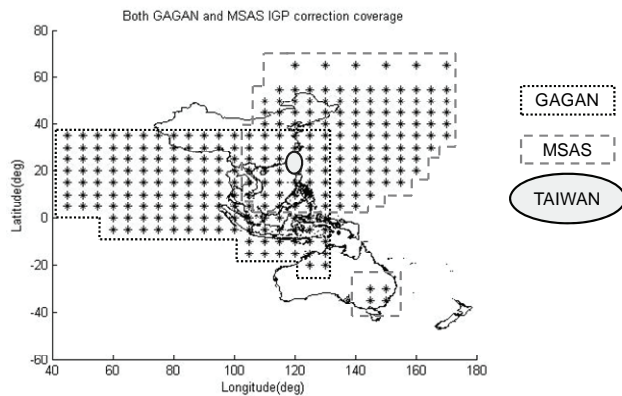


Figure 1 The possible SBAS service gap in Asia near Taiwan region [2]

This developed WADGNSS system has several Test-bed Reference Stations (TRSS) and one Test-bed Master Station (TMS). The TRSS used in this paper is the NLSC's e-GPS satellite tracking stations. These e-GPS satellite tracking stations are geographically distributed in Taiwan, and their coverage areas include the whole Taiwan region.

The TMS operation procedure includes the data collection, the TRSS process, the Common View Time Transfer (CVTT) [3], the ionospheric delay model estimation, the satellite orbit and clock error estimation, and the correction message packaging. The TRSS process of the TMS algorithm excludes the extraordinary data, then smoothes the pseudorange data from each TRS, and it also utilizes Weight Least Square (WLS) to estimate the clock error from each TRS. After that, the CVTT will use these results to synchronize the reference station oscillators. Moreover, the Kalman filter and the Chi-square test are employed to avoid the discontinuous data and to ensure the integrity in CVTT. The ionospheric delay model used in the paper is the thin shell ionospheric delay model which followed the WAAS Minimum Operational Performance Standards (MOPS) [4]. The final step of the master station is to produce the corrections for the orbit and clock errors for each satellite. The Minimum-Variance method and Kalman filter are applied to estimate the satellite orbit correction, and the satellite clock correction is calculated by WLS and Kalman filter [3]. This paper is mainly focus on the analysis of the TRS process and the CVTT because there are less papers on these two techniques. The overall

architecture of the WADGNSS TMS algorithm is shown in the Figure 2. The algorithms of all steps will be discussed in the following sections.

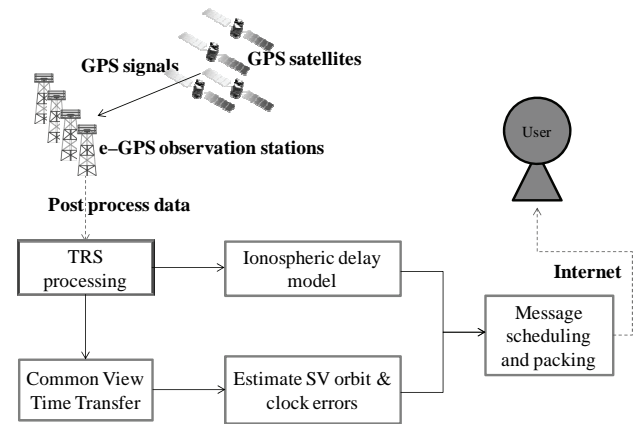


Figure 2 The flowchart of the WADGNSS master station algorithm

II. DATA COLLECTION

This paper tries to adopt the existing GPS reference stations which are originally designed for other applications, and the e-GPS satellite tracking stations are used as the TRSS in this paper. The e-GPS satellite tracking stations are developed and operated by the NLSC of Ministry Of the Interior (MOI) in Taiwan. They are originally designed for the geodetic surveying applications. As a result, it would be very challenging to use them as TRSS. First, the transmitted data format is not designed for the WADGNSS application, and the data format of e-GPS satellite tracking station is RTCM v3.0 for real time transmission and it is in RINEX for the post-process. However, the designate data format for our WADGNSS design is the National Satellite Test Bed (NSTB) data format [1]. To solve this problem, a transformation process between these data formats should be included. Considered there are more than 70 e-GPS satellite tracking stations which are geographically distributed over Taiwan region, the selections of the numbers of TRSS and their geometric distributions will influence the performance of the WADGNSS. Figure 3 shows the TRSS distribution used in this paper. This paper chooses only four reference stations as our approach because the limited computation load we can afford. Furthermore, Taiwan is a relative small island, therefore, four stations might be sufficient for a good geometric distribution. In this paper, the Taichung, Kaohsiung, Longdong, and Fugang stations are used as the TRSS in Taiwan.

III. TRS PROCESS

Among all the procedures in the TMS, the first step is the TRS process which is to handle the raw receiver data from one TRS, in the other words, each step of the

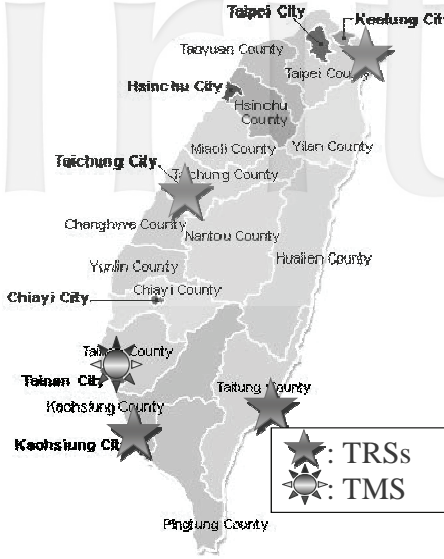


Figure 3 The TRSs distribution used in this paper

TRS process is not correlated with others TRSs. This TRS process includes the following estimations: the tropospheric delay, the ionospheric delay, the pseudorange residual and their variances for each satellite in view. Furthermore, the reference station clock state is also calculated. The code (PR) pseudoranges and carrier (ϕ) measurements on GPS L1 (1575.42MHz) and L2 (1227.6MHz) frequencies can be expressed as:

$$PR_{L1} = \rho_i^j + b_i - B^j + I_{i,L1}^j + T_i^j + v_{i,L1}^j \quad (1)$$

$$PR_{L2} = \rho_i^j + b_i - B^j + \gamma I_{i,L2}^j + T_i^j + v_{i,L2}^j \quad (2)$$

$$\phi_{L1} = \rho_i^j + b_i - B^j - I_{i,L1}^j + T_i^j + N_1 \lambda_1 + e_{i,L1}^j \quad (3)$$

$$\phi_{L2} = \rho_i^j + b_i - B^j - \gamma I_{i,L2}^j + T_i^j + N_2 \lambda_2 + e_{i,L2}^j \quad (4)$$

$$\gamma = \left(\frac{L_1}{L_2} \right)^2 = \left(\frac{1575.42}{1227.6} \right)^2 = 1.647 \quad (5)$$

where ρ_i^j is the true range between the j^{th} satellite and the i^{th} reference station receiver, b_i is the receiver clock bias, B^j is the satellite clock bias, $I_{i,L1}$ is the ionospheric delay on GPS L1 frequency, T is the tropospheric delay, $N_1 \lambda_1$ and $N_2 \lambda_2$ are the integer ambiguities in the carrier-phase measurements, and the e and v are the receiver noises in pseudorange (code measurement) and carrier-phase measurement, respectively. The main objective of the TRS process is to remove these errors, and generate a clean pseudorange residue to estimate the ionospheric delay model and satellite orbit and clock errors. The block diagram of the TRS process is summarized in Figure 4. The details of each step are described in the subsections below.

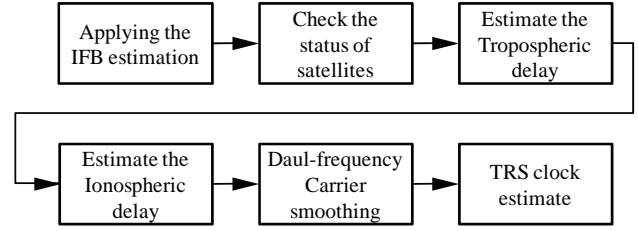


Figure 4 The block diagram of the TRS process

3.1 Applying the Inter-Frequency Bias (IFB) estimation

Because of the TRSs are using the L1-L2 dual-frequency receiver, the IFB could be a problem if no proper process has been taken [3]. Additionally, IFB must be estimated before we proceed to the TRS process. It is important to note that the IFB estimation of a TRS just needs once a life time. The IFB estimation used in this paper is derived from our prior project.

3.2 Check the Status of Satellites

The objective of this step is to select the healthy satellites for the future data processing. In this paper, checking whether the status of a satellite is healthy or not can be divided into three parts: 1) To check the satellite elevation angle. If the elevation angle of a satellite is lower than 5 degree, this satellite will be flagged as unhealthy. 2) To check the Signal to Noise Ratio (SNR) on L1 and L2 frequencies. The quality of this signal is positively related to its SNR. Thus if the SNR is below the threshold, this satellite is also flagged as unhealthy. The threshold value used in this paper is depended on the elevation angle. 3) To check that both L1 and L2 data has code phase data and carrier phase data. The Doppler velocity and pseudorange of a healthy measurement will be located at a certain range. Doppler velocity must be smaller than ± 10000 (meters per second), and pseudorange must be smaller than 10 to 4.5×10^7 (meters). If a satellite could pass above three tests, it can be declared as a healthy satellite. The comparison of positioning results between using all satellites in-view and the selected healthy satellites is shown in Figure 5. The y-axis is the Root Mean Square Error (RMSE) of positioning result. The red points are the positioning result using all satellites in-view, and the blue points are using the selected healthy satellites. It is obvious that the declared unhealthy satellites degrade the positioning performance. Therefore, it is a necessary step to eliminate the unhealthy satellites in the WADGNSS master algorithm.

3.3 Estimate the Tropospheric Delay

The tropospheric delay model and mapping function used in this paper are the Saastamoinen model [5] and Black Eisner troposphere formula [6], respectively. Subsequently, the tropospheric delays of all satellites' pseudoranges could be calculated. Figure 6 is the positioning result of using the tropospheric-free pseudorange. In Figure 6, the green points are positioning result while eliminating the estimated

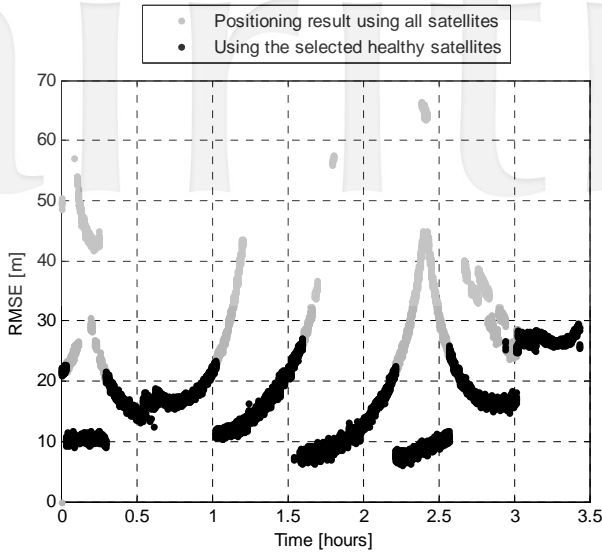


Figure 5 The comparison of positioning results between using all satellites in-view and the selected healthy satellites

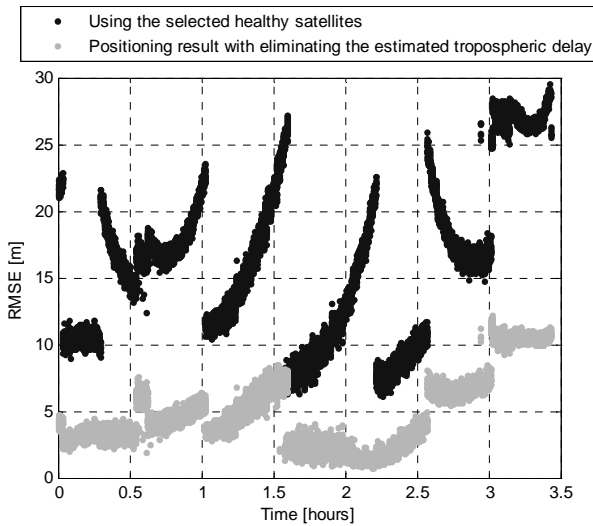


Figure 6 The positioning result of using the tropospheric-free pseudorange

tropospheric delay, and blue points are positioning result for the previous step (step B).

3.4 Smoothing of Pseudoranges and Ionospheric Delays

This step focuses on the dual-frequency carrier smoothing of pseudoranges and estimating the ionospheric delays. This paper utilizes the Hatch filter with little modification as the smoothing filter because of its simplicity [7]. This ionospheric Hatch filter is to implement the Hatch filter to estimate the smoothed ionospheric delay by the code and carrier measurements of the ionospheric delays. The block diagram of the ionospheric Hatch filter is shown in Figure 7.

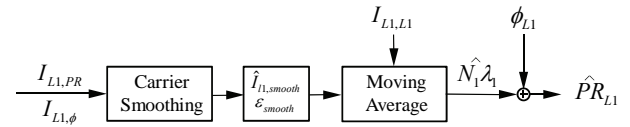


Figure 7 The block diagram of the ionospheric Hatch filter

The calculations of the code and carrier ionospheric delays are shown in Equation (6) and Equation (7).

$$I_{L1,PR} \equiv \frac{PR_{L2} - PR_{L1}}{\gamma - 1} = I_{L1} + v_{PR} \quad (6)$$

$$I_{L1,\phi} \equiv \frac{\phi_{L1} - \phi_{L2}}{\gamma - 1} = I_{L1} + Amb + v_{\phi} \quad (7)$$

$$I_{L1,L1} \equiv \frac{PR_{L1} - \phi_{L1}}{2} = I_{L1} + \frac{N_1 \lambda_1}{2} + v_{L1} \quad (8)$$

where I_{L1} is the ionospheric delay on L1 frequency, $I_{L1,PR}$ is the combination of code phase measurement, $I_{L1,\phi}$ is the combination of carrier phase measurement. Amb is the combination integer ambiguity for carrier phase, and v is the noise. Noise v includes the multipath and receiver thermal noise error. The order is: $v_{PR} > v_{L1} > v_{\phi}$. $N\lambda$ is the integer ambiguity. Because of the Amb , v_{PR} , v_{L1} , and v_{ϕ} , the ionospheric delays calculated in (6) and (7) are not accurate. In order to reduce these errors, the dual-frequency carrier smoothing technique for pseudoranges and ionospheric delays is used in the ionospheric Hatch filter. After the smoothing technique, the smooth $\hat{I}_{L1,smooth}$ is considered as a result of the estimated ionospheric delay. The second step is to apply the moving average filter to combine $I_{L1,L1}$ and $\hat{I}_{L1,smooth}$ to estimate the $N\lambda$ [8]. From (8), it can be re-written as (9) as below. In (9), W_1 and W_2 are the weighting of GPS L1 carrier bias and the weighting of ionospheric GPS L1 carrier bias, respectively [7].

$$-\frac{N\lambda}{2} = (W_1 * b_{L1} + W_2 * (I_{L1,L1} - I_{L1,PR})) / (W_1 + W_2) \quad (9)$$

After calculating the integer ambiguity, the smoothed pseudorange could be obtained. Moreover, the ionospheric delays for all satellites are calculated in the ionospheric Hatch filter, and these results will be used in the step of generating the correction of the Ionospheric Grid Point (IGP).

The positioning result using the smoothed pseudorange that generated by the ionospheric Hatch filter is show in Figure 8. Figure 8 also shows the comparison of positioning results between the one of the previous step and the one after implementing the ionospheric Hatch filter. In Figure 8, one notes that the positioning results of the smoothed pseudorange become smoother and therefore more accurate.

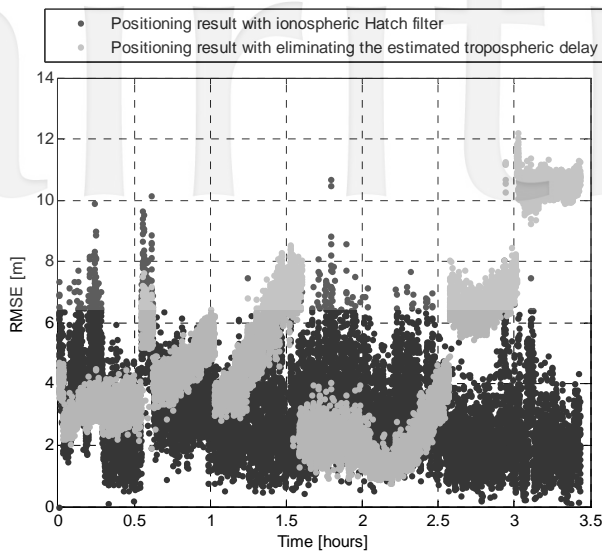


Figure 8 The positioning result after implementing the ionospheric Hatch filter

3.5 TRS Clock Estimate and TRS Process Result Analysis

This paper uses the WLS to estimate each TRS clock error and its variance. Furthermore, the Chi-square test [9] is utilized to check the result, and the Student's T test is used to detect and isolate the outlier [10].

Figure 9 shows the positioning results of each TRS process step, and Table 1 lists the standard deviations of the position errors in the ENU coordinate for each step in TRS process. As indicated in Figure 9 and Table 1, one notes that the TRS process has great capability of estimating a clean and smoothed pseudorange of each reference station, and this smoothed pseudorange is an ionospheric error free and tropospheric error free measurement. In the other words, the TRS process can estimate the tropospheric delay, the ionospheric delay, the pseudorange residuals and their variances, and TRS process also obtains the satellite position, the obliquity factor, the ionospheric pierce point location, the elevation angle, the azimuth angle, and the station clock. All of these parameters are calculated for the rest of procedures of the TMS algorithm.

IV. COMMON VIEW TIME TRANSFER

The synchronization of the TRSs clock by the Common View Time Transfer (CVTT) technique will be discussed in this section. Each TRS has its own oscillator to offer a stable time. However, every TRS oscillator will be affected by the environment which means that the reference station clock error would not be the same. If the TRS clocks are not synchronized, the satellite orbit and clock correction can't be generated. Because if TRSs are not synchronized, the difference between the pseudorange residual for the same satellite with different TRS will include the non-synchronized error. In that way, the satellite orbit and clock error

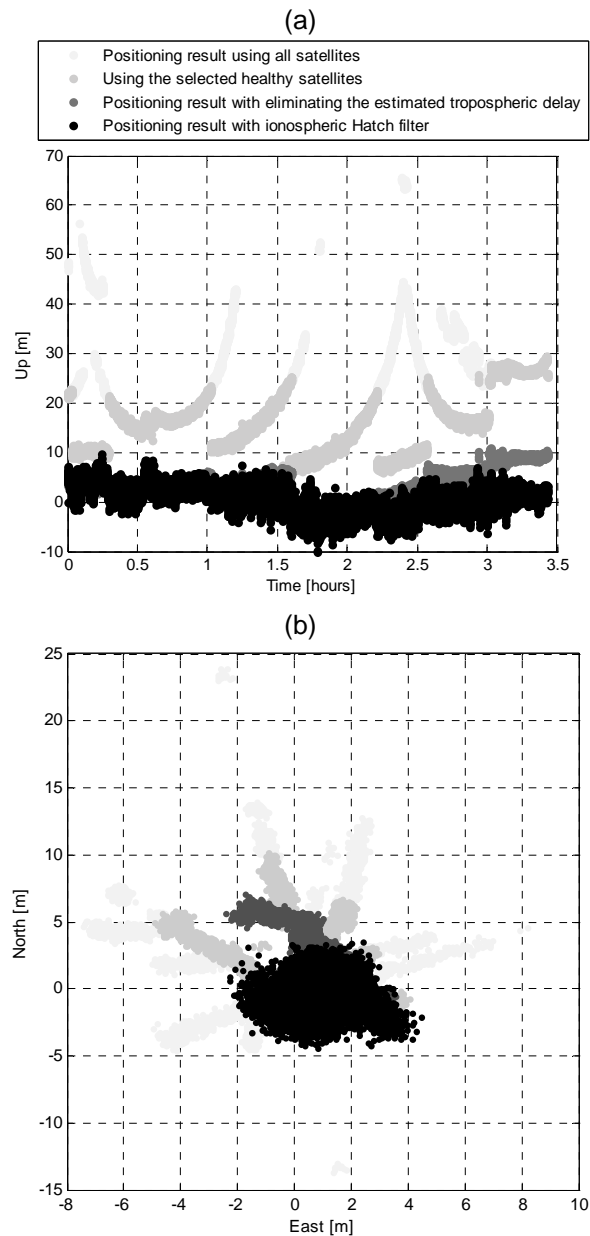


Figure 9 The position errors in the ENU coordinate for different stages of TRS process. Plot (a) is the vertical error, and plot (b) is the horizontal error.

Table 1 Standard deviations of positioning errors (in meter) for different stages of TRSs process

Each step of TRS processing	East std (m)	North std (m)	Up std (m)
Raw GPS	2.3907	3.6051	9.6848
Confirm the health status of satellites	1.5079	2.2351	5.7467
Tropospheric delay free	0.7397	1.6664	3.1834
Smoothing pseudorange & ionospheric delays free	0.9121	1.2972	2.7319

cannot be separated. Equation (10) shows the ionospheric-free and tropospheric-free pseudorange. The true range ρ_i^j in (11) is divided into $\hat{\rho}_i^j$ and $\Delta r^j * 1_i^j$, where $\hat{\rho}_i^j$ is a range that calculated by a known reference position and a estimated satellite position. $\Delta r^j * 1_i^j$ is the satellite orbit error in the light of sight vector. The measurement in (12) is the defined pseudorange residual. The definition of this pseudorange residual is that the ionospheric-free and tropospheric-free pseudorange minus the range between the known reference position and the estimated satellite position.

$$\Pr_{i,smoothed,iono-free,trop-free}^j = \rho_i^j + b_i - B^j + v \quad (10)$$

$$\Pr_{i,smoothed,iono-free,trop-free}^j \equiv (\hat{\rho}_i^j + \Delta r^j \cdot 1_i^j) + b_i - B^j + v \quad (11)$$

$$\begin{aligned} \delta \Pr_i^j &= \Pr_{i,smoothed,iono-free,trop-free}^j - \hat{\rho}_i^j \\ &= \Delta r^j \cdot 1_i^j + b_i - B^j + v \end{aligned} \quad (12)$$

The purpose of CVTT is to synchronize all TRS clock error in pseudorange residual from each TRS. The CVTT technique can be divided into two stages: 1) To estimate the difference between two TRS clock errors and its variance. 2) To choose a reference station clock as the master clock and to synchronize the rest of TRSs with it.

The purpose of the first stage is to calculate the relative reference station clock error between two stations and to provide this result to the next stage. Moreover, it also finds the common view satellites between two TRSs. The equations to calculate the relative clock bias are shown in (13) and (14): where $\Delta_{m,M}^j$ is the difference between two TRSs pseudorange residuals for the same satellite, $(I_m^j - I_M^j)$ is the line of sight difference, $\Delta \hat{b}_{m,M}$ is the clock bias difference, $v_{m,M}^j$ is the noise, and $K_{m,M}$ is the number of satellites in common view for both TRSs. Because $(I_m^j - I_M^j)$ and $v_{m,M}^j$ are of very small values, a good estimation of the clock difference can be achieved as depicted in (14). Finally, this paper uses the Kalman filter to avoid the discontinuous situation and to calculate a smoothed relative clock bias.

$$\Delta_{m,M}^j = \delta \Pr_m^j - \delta \Pr_M^j = \Delta r^j \cdot (1_m^j - 1_M^j) + \Delta \hat{b}_{m,M} + v_{m,M}^j \quad (13)$$

$$\Delta \hat{b}_{m,M} = \frac{1}{K_{m,M}} \sum_{j=1}^{K_{m,M}} (\Delta_{m,M}^j) \quad (14)$$

In the second stage, the purpose is to calculate the synchronized TRS clock bias. This stage is to find the first healthy TRS, and regard it as the master clock. The pseudorange residual of the chosen master clock TRS

will eliminate its own clock bias which was estimated from the previous TRS process. The other TRSs synchronize to the master clock by the relative clock difference we obtained at the first stage. The calculations of the relative clock bias, the pseudorange residual without relative synchronized clock bias and its variance can be expressed as:

$$\delta \Pr_m^j = \delta \Pr_i^j - \Delta \hat{b}_{m,M} - \Delta \hat{b}_M = \Delta r^j \cdot 1_i^j - B^j + v \quad (15)$$

$$\sigma_{\Pr_m}^2 = \sigma_{\delta \Pr_m}^2 + \sigma_{\Delta \hat{b}_{m,M}}^2 + \sigma_{\Delta \hat{b}_M}^2 \quad (16)$$

The pseudorange residuals before and after CVTT are shown in Figure 10. It is important to note that before applying CVTT, pseudorange residual varies with time. Because TRS receiver oscillator will automatically adjust its clock bias, we can find the green line has a sudden change around 300 epoch. After the CVTT process, the pseudorange residuals will not change with the receiver clock, and it becomes a very small value.

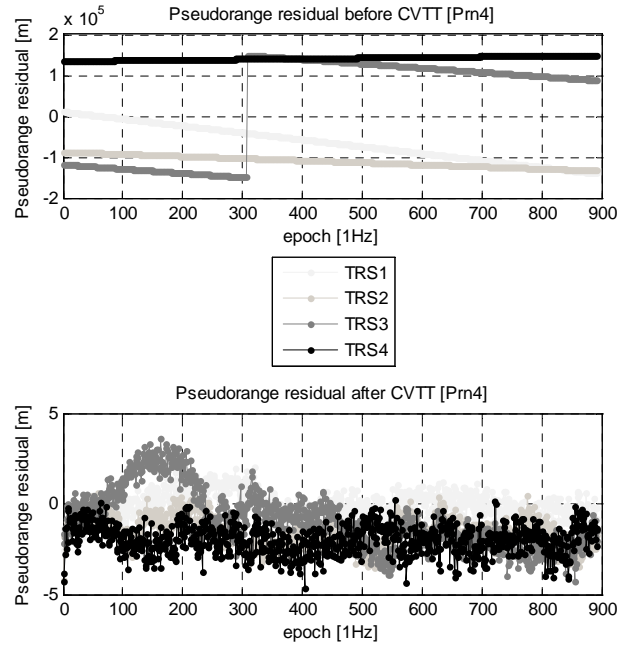


Figure 10 The calculated pseudorange residuals before and after applying CVTT for four TRSs

After the CVTT process, the measurements from all the TRSs are synchronized, therefore, the satellite orbit and clock correction can be estimated.

V. ESTIMATE SATELLITE ORBIT AND CLOCK ERROR

The CVTT process is very important because the measurements are decoupled from one satellite to other

satellite [11-12]. After the TRS process and CVTT, the pseudorange residuals which effect the positioning solutions are the satellite clock and orbit error. Before estimating the satellite ephemeris and clock error, the satellite ephemeris and clock measurement must be separated first. The ephemeris and clock corrections do not need to update at the same time, because the satellite clock correction update more frequently. Separating ephemeris error and clock error estimation can reduce the computation of the whole TMS process. Figure 11 illustrates the process of the satellite orbit correction computation.

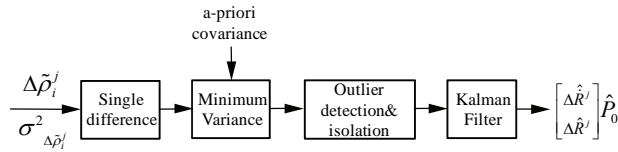


Figure 11 The block diagram of the satellite orbit correction computation

In order to separate the satellite clock and orbit error, this paper uses the pseudorange residual which is synchronized with all TRSs to do the single difference. As shown in (17), the satellite clock B^j will be eliminated.

$$\Delta\tilde{\rho}_i^j - \Delta\tilde{\rho}_m^j = \Delta r^j \cdot (I_i^j - I_m^j) + \varepsilon_i^j \quad (17)$$

where the subscript m represents the TRS which has the Minimum-Variance (MV) [13], and Δr^j is the unknown satellite orbit error. Equation (17) also can be changed as:

$$Z = H \cdot \Delta r^j + v \quad (18)$$

where

$$Z = \begin{bmatrix} \Delta\tilde{\rho}_1^j - \Delta\tilde{\rho}_m^j \\ \vdots \\ \Delta\tilde{\rho}_{N-1}^j - \Delta\tilde{\rho}_m^j \end{bmatrix}, H = \begin{bmatrix} I_1^j - I_m^j \\ \vdots \\ I_{N-1}^j - I_m^j \end{bmatrix}, \text{cov}(v) = W$$

v is the noise, and N is the TRS number which was synchronized. Z and H are matrixes consist of $N-1$ measurements. The average of v is 0, and the variance is W . MV is used to estimate satellite orbit error in this paper. Because of the number of satellites tracked by TRSs will be changed when the satellites move, (18) may be under-determined or over-determined. MV can satisfy these two situations [13-14]. The state vector x will be symbolized as unknown satellite orbit error in the following statement. The following statement will use the state vector x to stand for the unknown satellite error. By using the value obtained at the previous second, Λ and W can be determined by using the cost function of MV as shown in (19) and (20) [13-14]:

$$\hat{x}_{MV} = (\Lambda^{-1} + H^T W^{-1} H)^{-1} H^T W^{-1} z \quad (19)$$

$$\begin{aligned} \hat{P}_{mv} &= E[(x - \hat{x}_{MV})(x - \hat{x}_{MV})^T] \\ &= (\Lambda^{-1} + H^T W^{-1} H)^{-1} H^T W^{-1} H (\Lambda^{-1} + H^T W^{-1} H)^{-1} \\ &= (\Lambda^{-1} + H^T W^{-1} H)^{-1} \end{aligned} \quad (20)$$

According to the matrix inversion lemma, equation (19) and (20) can be rewritten as (21) and (22) [15]. Subsequently, the satellite orbit correction has been calculated.

$$\hat{x}_{MV} = \Lambda H^T (H \Lambda H^T + W)^{-1} z \quad (21)$$

$$\hat{P}_{mv} = \Lambda - \Lambda H^T (H \Lambda H^T + W)^{-1} H \Lambda \quad (22)$$

After generating the satellite orbit correction, next is to compute the satellite clock correction. The satellite clock correction can be obtained by using the satellite orbit correction result and the pseudorange residual as:

$$Z_{c,i}^j = \Delta\hat{r}^j \cdot I_i^j - \Delta\tilde{\rho}_i^j = \Delta B^j + n_{c,i}^j \quad (23)$$

$$\sigma_{c,i}^j{}^2 = I_i^j{}^T \cdot \hat{P}_3 \cdot I_i^j + \sigma_{\Delta\tilde{\rho}_i^j}^2 \quad (24)$$

where \hat{P}_3 is the covariance of the upper triangular matrix, which is generated by the calculation of the satellite orbit correction. The dimension is 3×3 . Then rewrite (24) in the matrix form:

$$Z_c = H_c \Delta B^j + n_c \quad (25)$$

H_c is composed by the unit row vector, whose dimension is the number of observations * 1, n_c is the noise of observations, the covariance matrix (W_c) of the diagonal elements is provided by (24). Finally, we use WLS to estimate the satellite clock error as

$$\Delta\hat{B}_{WLS}^j = (H_c^T W_c^{-1} H_c)^{-1} H_c^T W_c^{-1} Z_c \quad (26)$$

$$\hat{P}_c^j = (H_c^T W_c^{-1} H_c)^{-1} \quad (27)$$

Figure 12 summaries the process of generating the satellite clock correction. In order to avoid the outlier influencing the estimation result, WLS and outlier detection is utilized. Finally, this paper uses the Kalman filter to calculate the satellite clock correction.

Figure 13 illustrates the corrections for the satellite orbit and clock error.

VI. IONOSPHERIC DELAY MODEL

Although the ionospheric delay has been calculated at the TRS process stage, that ionospheric delay estimate can only be applied to the TRS instead of users. In

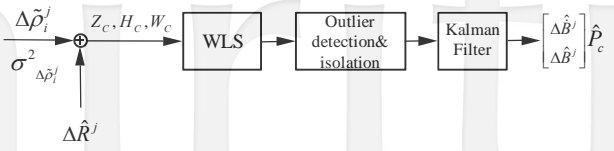


Figure 12 The block diagram of the satellite clock correction computation

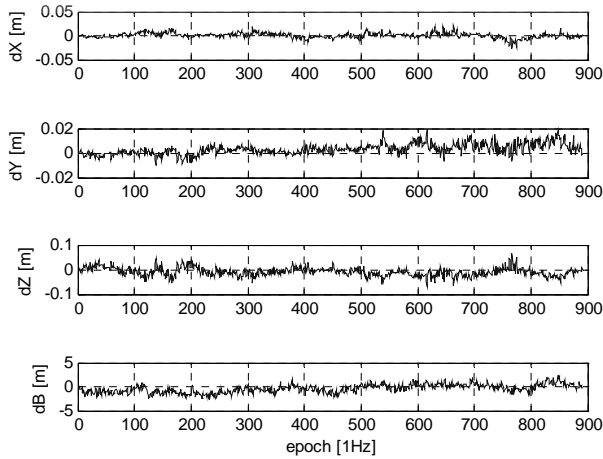


Figure 13 Corrections for PRN 2 satellite orbit and clock error

order to offer users the ionospheric delay correction, an ionospheric delay model must be utilized. Users under the WADGNSS coverage region can apply the ionospheric delay model to calculate their own ionospheric correction.

Figure 14 shows the flow chart of the calculation for the user ionospheric delay correction. First of all, TRS process estimates the ionospheric slant delay on Ionospheric Peirce Point (IPP) and uses the satellite elevation angle to calculate the Obliquity Factor (OF) [3] as shown in (27):

$$OF = \frac{\text{slant delay}}{\text{vertical delay}} = \left\{ 1 - \left[\frac{R_e}{R_e + h} \cos(el) \right]^2 \right\}^{-\frac{1}{2}} \quad (27)$$

Then using OF to calculate the vertical ionospheric delay on IPP as shown in (28):

$$I_{\text{vertical}} = \frac{I_{\text{slant}}}{OF} \quad (28)$$

Then take the vertical ionospheric delay on IPP into WLS to accumulate and generate the vertical ionospheric delay for each Ionospheric Grid Point (IGP). Subsequently, users receive GPS signal and the WADGNSS message, and users can apply the vertical ionospheric delay on IGPs to estimate the vertical ionospheric delay on each of their IPP. Finally, using the OF to compute the slant ionospheric delay.

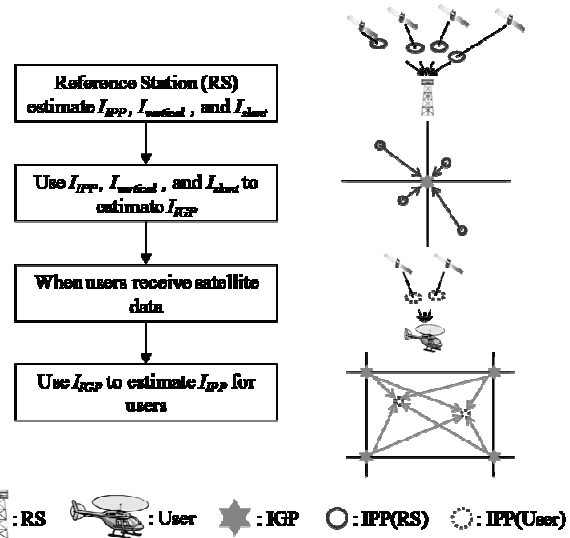


Figure 14 The flow chart of the calculation for the user ionospheric delay correction

For the general L1 single frequency users, they can use Klobuchar model to reduce about 60% of the ionospheric error [16-17]. This Klobuchar model uses eight parameters to represent the ionospheric spatial and temporal changes, it assumes that the ionosphere effect small in the evening. Then use cosine function to approximate the daytime ionosphere correction. Finally, substitute the ionosphere correction into the IPP location. It can be obtained Klobuchar ionospheric correction.

Figure 15 shows the final positioning results comparison: the blue line is using the stand alone GPS, and the red line is using the WADGNSS ionospheric delay model. Furthermore, the red line shows the result for satellites with the ionospheric correction to do positioning.

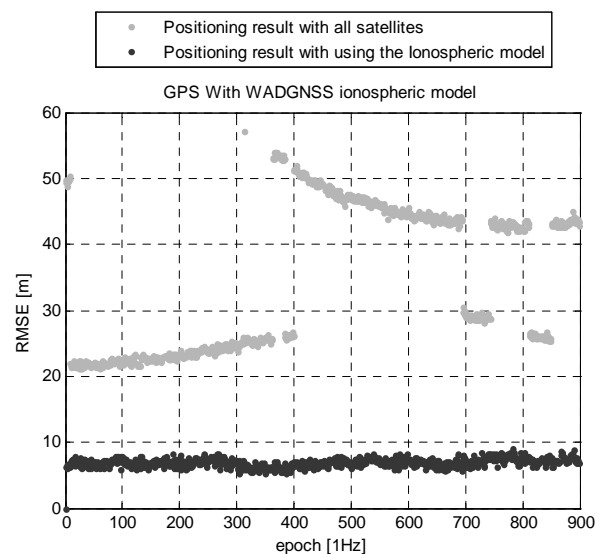


Figure 15 positioning result Comparison: using stand alone GPS and using the WADGNSS ionospheric delay model

VII. CONCLUSIONS AND FUTURE WORK

This paper developed a Wide Area Differential GNSS (WADGNSS) that is a GNSS augmentation system for Taiwan region. The goal of this WADGNSS is to provide a positioning service which meets the required navigation performance: namely accuracy, integrity, continuity and availability. The complete WADGNSS master station algorithm was illustrated in this paper. Moreover, the real GPS data collected from e-GPS satellite tracking stations were used to validate each TMS process step. By these results, the improvement on positioning performance gained from the TMS process can be observed by comparing the positioning results with stand-alone GPS to that of the WADGNSS. As a result, the WADGNSS master station algorithm was successfully implemented and demonstrated in this paper. The next step is to extensively test the integrity of the implemented WADGNSS for possible applications.

ACKNOWLEDGEMENT

The work presented in this paper is supported by Taiwan National Land Surveying and Mapping Center. The authors gratefully acknowledge the supports.

REFERENCES

- [1] Fuller, R. A., *Aviation Utilization of Geostationary Satellites for the Augmentation to GPS: Ranging and Data Link*, Department of Aeronautics and Astronautics Thesis, Stanford University, 2000.
- [2] Chen, C. H., *GPS Performance Assessment of a Local Area Monitoring System in Taiwan Region*, Department of Aeronautics and Astronautics Thesis, National Cheng Kung University, 2008.
- [3] Chao, Y. C., *Real Time Implementation of the Wide Area Augmentation System for the Global Positioning System with an Emphasis on Ionospheric Modeling*, Department of Aeronautics and Astronautics Thesis, Stanford University, 1997.
- [4] WAAS MOPS (Minimum Operational Performance Standards for global positioning system/ Wide Area Augmentation System airborne equipment), RTCA/DO-229D.
- [5] Saastamoinen, J., Contributions to the theory of atmospheric refraction, In three parts: Bulletin Géodésique, 1973, No. 105, pp. 270-298; No. 106, pp. 383- 397; No. 107, pp. 13-34.
- [6] Black, H.D., "An Easily Implemented Algorithm for the Tropospheric Range Correction," *Journal of Geophysical Research*, Vol. 83, No. B4, April 1978.
- [7] Hatch, R. R., "The Synergism of GPS Code and Carrier Measurements," *Proceedings of the Third Geodetic Symposium on Satellite Doppler Positioning*, Las Cruces, NM, Feb 1982, pp123-1232.
- [8] Chao, Y. C., Tsai, Y. J., Walter, T., and Kee, C., "The Ionospheric Delay Model Improvement for the Stanford WAAS Network," *Proceedings of ION National Technical Meeting 95*, Anaheim, California, January 1995.
- [9] Sanders, M. A., "Characteristic function of the central chi-square distribution," Retrieved, 2009, <http://www.planetmathematics.com/CentralChiDistr.pdf>
- [10] Press, William H., Saul A., Teukolsky, William T. Vetterling, and Brian, P. Flannery, *Numerical Recipes in C: The Art of Scientific Computing*, Cambridge University Press, 1992.
- [11] Kee, C., *Wide Area Differential GPS (WADGPS)*, Department of Aeronautics and Astronautics Thesis, Stanford University, 1993.
- [12] Schempp, T., Burke, J., and Rubin, A., "WAAS Benefits of GEO Ranging," *Proceedings of ION-GNSS 21st. International Technical Meeting*, Savannah Georgia, Sept. 2008.
- [13] Tsai, Y. J., Chao, Y. C., Walter, T., and Kee, C., "Evaluation of Orbit and Clock Models for Real-Time WAAS," *Proceedings of the National Technical Meeting*, The Institute of Navigation, Anaheim, California, 1995.
- [14] Tsai, Y. J., *Wide Area Differential Operation of the Global Positioning System: Ephemeris and Clock Algorithms*, Department of Aeronautics and Astronautics Thesis, Stanford University, 1999.
- [15] Alvarado, F. L., "The Matrix Inversion Lemma," The University of Wisconsin Madison, Wisconsin, 53706, USA, March 1999.
- [16] Klobuchar, J. A., "Design and Characteristics of the GPS ionosphere Time Delay Algorithm for Single Frequency Users," *Proceeding of IEEE Position Location and Navigation Symposium*, Las Vegas, NV, 1986.
- [17] Parkinson, B. W. and Spilker J. J., *Global Positioning System: Theory and Application*, American Institute of Aeronautics and Astronautics, 1996.